On the full topology of the Laplacian of the electron density II: Umbrella inversion of the ammonia molecule

ARTICLE *in* THE JOURNAL OF PHYSICAL CHEMISTRY A · AUGUST 2001

Impact Factor: 2.69 · DOI: 10.1021/jp0013937

On the Full Topology of the Laplacian of the Electron Density II: Umbrella Inversion of the Ammonia Molecule

Nathaniel O. J. Malcolm and Paul L. A. Popelier*

Department of Chemistry, U.M.I.S.T., 88 Sackville Street, Manchester M60 1QD, UK

Received: April 12, 2001; In Final Form: May 24, 2001

The full topology of $L(\mathbf{r})$, which is defined as minus the Laplacian of the electron density, $\nabla^2\rho$, has recently been explored for the water molecule (*Coord. Chem. Rev.* **2000**, *197*, 169). In this work, we have investigated the changing topology during the "umbrella" inversion in ammonia. The maxima in $L(\mathbf{r})$ are points of local charge concentration, which can be associated with the electron pairs of VSEPR theory. We examine changes in three valence shell charge concentration (VSCC) and three depletion (VSCD) graphs as a function of the angle between the C_3 axis and a hydrogen. Through the use of planar graphs, the transition mechanisms can be easily rationalized. The previously noted double maxima in $L(\mathbf{r})$, corresponding to the lone-pair of nitrogen, found at the transition state for inversion is shown to persist for geometries distorted considerably from planar. The transitions between structures in the valence shell charge concentration and charge depletion graphs do not occur simultaneously.

1. Introduction

In recent years, the so-called topological approach has become an increasingly popular tool[1] in providing a mathematical bridge between chemical intuition and quantum mechanics. The roots of this approach lie in the pioneering work of the Bader group, which culminated in a formulation of subspace quantum mechanics known as the theory of "Atoms in Molecules" (AIM).[2,3] One of the key features of the topological approach is that the gradient vector field of a 3D function partitions real space into quantum subsystems, bounded by surfaces known as separatrices. This fact was first realized in the 1970s[4] and led to the development of AIM, which identified the subsystems with chemical atoms. The topology of the electron density ρ is better understood than that of other 3D functions, such as the Laplacian of the electron density, $\nabla^2\rho$, or the Electron Localization Function (ELF).[5] Indeed, because ρ was the first function to be studied by the topological approach most algorithms have focused on it as witnessed by current atomic integration algorithms.[6−8] However, more 3D fields are being subject to a topological analysis, such as the virial field,[9] magnetically induced molecular current distributions,[10] or the intracule density.[11] This expansion expresses the need for generalized software, enabling a systematic topological analysis of future fields and current topologically unanalyzed fields, such as the Localized Orbital Locator (LOL)[12] or the Lennard−Jones Function (LJF).[13]

The idea of using the gradient vector field to retrieve chemical information from wave functions has since been demonstrated by a sizable and growing number of publications.[1] In the 1980s, $\nabla^2\rho$ became the second 3D function to be analyzed in terms of the topological approach.[14] However, this analysis was restricted to the localization and characterization of critical points (CPs), i.e., points where the gradient of the field vanishes. An analysis of the Laplacian's CPs proved useful in the prediction of sites of electrophilic and nucleophilic attack, as well as their relative propensity toward reaction,[15] the structures and geometries of hydrogen-bonded complexes,[16] the directing abilities of substituents in aromatic electrophilic substitution[17] and the relative susceptibility of activated double bonds to Michael addition.[18] These studies ultimately resulted in the formulation of a Laplacian complementarity principle.[19] Perhaps one of the most important applications of the topology of the Laplacian is the construction of a physical basis for the well-known VSEPR model.[20−23] The correspondence between the Laplacian and the VSEPR model is subject to maintained scrutiny,[24] especially in connection with transition metals.[25−28] Recently, great progress[29] has been made in taking the aforementioned correspondence beyond empirical observations by studying the mapping of the conditional pair density onto the electron density. In summary, the Laplacian is a conceptually simple function that clearly contains a wealth of information and continues to contribute to the elucidation of chemical shape and behavior.

Another more involved function that has been met with considerable attention is ELF. Silvi and Savin were the first to investigate its topology.[30] Their seminal paper piloted a host of applications including a delocalization criterion for unsaturated carbon bonds,[31] and aromatic, antiaromatic, hypervalent, and hydrogen-bonded molecules,[32] a characterization of hydrogen bonds of various strengths,[33] the determination of protonation sites in bases,[34] an analysis of depleted homopolar bonds,[35] a representation of the metallic bond[36] and a structural characterization of lathanide trihalides.[37] Changes in ELF's topology upon nuclear displacement were first considered by Silvi et al.[38] This "dynamic" study introduced their Bonding Evolution Theory following Bader's application[39] of Thom's catastrophe theory[40] in the context of the electron density. Subsequently, several dynamic ELF studies appeared, comprising the proton transfer in $H_5O_2^+$,[41] an analysis of electrophilic aromatic substitution,[42] bonding in hypohalous acids,[43] structure and bonding of chlorine oxides and peroxides,[44] the isomerization mechanism in XNO,[45] and electron transfer in the Li + Cl_2 system.[46]

It is the purpose of this paper to further study the full topology

* To whom correspondence should be addressed. E-mail: n.malcolm@umist.ac.uk, pla@umist.ac.uk. Fax: 44−161−200 4559.

10.1021/jp0113937 CCC: $20.00
Published on Web 07/21/2001

of the Laplacian, or more precisely, $L(\mathbf{r}) = -\nabla^2\rho(\mathbf{r})$, which is more intuitive. In an earlier paper,[47] hence referred to as paper I, it was shown that $L(\mathbf{r})$ contains as many as 43 CPs in a single water molecule. This large set of CPs can be divided into four subsets, by realizing that oxygen contains a core shell and a valence shell, each split into a charge concentration and a charge depletion part (see section 2). The topological connectivity of the CPs, as expressed by a graph, is the key to understand how they are interrelated. To the best of our knowledge, this is the first time that graphs, drawn from the CPs of $L(\mathbf{r})$, are investigated with respect to varying nuclear positions for polyatomic systems. A recent study has examined the changes in the electron density and it Laplacian in the formation of diatomic molecules.[48] Inspired by an early study on distorted amides[49] we decided to examine the inversion of NH_3. In particular, we were intrigued by the question how a single CP in $L(\mathbf{r})$, associated with a lone pair in an ammonia molecule with a pyramidal nitrogen, can split into two CPs in the planar ammonia with a flat nitrogen environment.

2. Theoretical Background

2.1 Some Topological Definitions. Because the use of topological concepts is well documented[2,3] we briefly review only a few key concepts here. Paths of steepest ascent through a scalar field *S* are called *gradient paths.* The gradient of the field *S*, ∇S, is everywhere tangent to a point on a gradient path. Gradient paths clearly have a sense: they originate and terminate at points in space where ∇S vanishes, termed *critical points* (CP). The collection of gradient paths is called a *gradient vector field*, which naturally partitions a molecule into subspaces called *basins.* A basin contains a CP, a maximum, at which the gradient paths that form the basin terminate.

In two dimensions, there can only be three types of CP: a maximum a minimum or a saddle point. In three dimensions, however, there are two types of saddle point, which are typified by the local curvature of the field at the CP. In a 3D function, the different CPs are characterized by eigenvalues of the Hessian of the field, evaluated at the CP, denoted by λ_i ($i = 1, 2, 3$). The *rank* (r) of a CP refers to the number of nonzero eigenvalues and the *signature* (s) to the sum of the signs of the eigenvalues. Hence, CPs are compactly designated by (r,s). Usually, one encounters only CPs of rank 3, i.e., those with strictly nonzero Hessian eigenvalues, leaving four types of CP.

2.2 Charge Concentration and Depletion. In the following, we set the scalar field to $L(\mathbf{r})$, and for more details the reader is referred to Paper I. It has been observed that the local maxima in $L(\mathbf{r})$ show a remarkable correspondence with the idealized electron-pairs[14] of the Lewis model. Using a finite difference formula, it is easy to prove[3] that when $L(\mathbf{r}) > 0$, the electron density is locally concentrated, and conversely when $L(\mathbf{r}) < 0$, the electron density is locally depleted. In summary, the fact that $L(\mathbf{r})$ gauges the concentration of ρ implies that it can be used to detect electron pair localization.

For a free atom, $L(\mathbf{r})$ is able to reveal the shell structure, but unlike ELF it is unable to reveal more than five atomic shells.[5] However, it has been observed that $L(\mathbf{r})$ is homeomorphic with the Laplacian of the conditional pair density.[29] The profile of $L(r)$, where r is the radial distance from the nucleus of a free spherical atom, contains zones corresponding to Charge Concentration (CC) ($L(r) > 0$) or Charge Depletion (CD) ($L(r) < 0$). The inner CC and CD zones are labeled the Core Shell Charge Concentration (CSCC) and Core Shell Charge Depletion (CSCD) zones. The outer CC and CD regions are called the Valence Shell Charge Concentration (VSCC) and Valence Shell Charge Depletion (VSCD) zones. For second period elements (Li→Ne) elements, these are the only four shells that can occur. An investigation of the complete shell structure of heavier elements (e.g., third period, transition metals) in chemical compounds may call for an extended nomenclature including the intermediate CC and CD shells. For many-electron atoms in their ground state the radius of the nodal sphere separating the CSCC and the CSCD is approximately 1/Z a.u. As a result, the core shell radius for free oxygen is about 0.13 au, whereas the corresponding radius for the valence shell (i.e., of the nodal sphere between the VSCC and the VSCD) is 0.91 au.[47] Thus, the core shell lies much deeper into the atomic shell structure than the valence shell.

As free atoms come together to form a molecule the topology of $L(\mathbf{r})$ displays CPs of rank three, which are linked via gradient paths in $L(\mathbf{r})$ to form graphs. It is convenient to associate one graph with each type of shell, for example the VSCC has its own graph, and so has the VSCD. Four such graphs (CSCC, CSCD, VSCC, VSCD) have been described in detail for water in paper I. The CS graphs have a much simpler structure than the VS graphs and are expected to be chemically less important than the VS graphs. In this work, we will concentrate entirely on the changes observed in the VSCC and VSCD graphs.

An important new aspect of the current series of papers is the presentation of full graphs for the charge concentration and depletion in $L(\mathbf{r})$. Previous studies of the Laplacian had concentrated on the location of the CPs.[50] Most arguments were developed through examination of the values of ρ and its Laplacian at the CPs.[14,17,19] This approach, though proving useful in some circumstances, is susceptible to errors due to potentially missing some CPs. The tracing of gradient paths from the (3, −1) and (3, +1) CPs results in a complete picture of the connectivity of the CPs. It is thus immediately apparent if any important CPs have been omitted.

2.3 Planar Graphs. The VSCC and VSCD graphs considered in this work can be represented and classified through the use of planar graphs.[19] A planar graph is defined as a graph that can be drawn in a plane without any of its edges crossing each other. It was shown in Paper I that the sub-graphs of $L(\mathbf{r})$ obey these rules. According to Euler[51] a planar graph obeys the following formula

$$V - E + F = 2 \tag{1}$$

where V, E, and F represent the number of vertexes, edges and faces in the planar graph, respectively. In the representation of the charge *concentration* graphs the vertexes are associated with the (3, −3) CPs, the edges with the (3, −1) CPs and the faces with the (3, +1) CPs. However, in the representation of the charge *depletion* graphs the vertexes are associated with the (3, +3) CPs, the edges with the (3, +1) CPs and the faces with the (3, −1) CPs. As an example, we reproduce the VSCC graph of the water molecule originally presented in Paper I in Figure 1. It is important to consider that the outside of the graph as a face, as well as the enclosed areas.

2.4 Structure vs Geometry. The theory of AIM makes a clear distinction between geometry and structure based on the topology of ρ.[3,52] The *geometry* of a molecular system is defined by the set of nuclear coordinates, denoted by $\mathbf{R}$, whereas the *structure* is determined by the connectivity of the molecular graph. The essential idea behind this distinction can be transferred to $L(\mathbf{r})$. More precisely, an infinitesimal change in coordinate values leads to a different geometry with coordinates $\mathbf{R}'$. In this work, a multitude of different ammonia geometries has been generated by changing a valence angle, defined below.

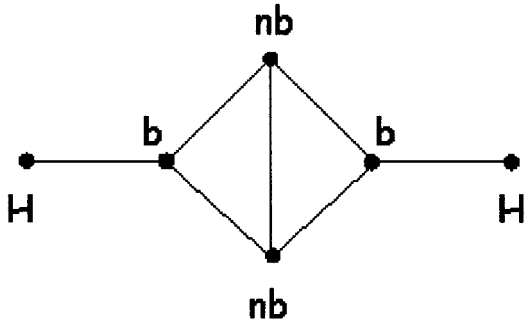

Figure 1. Planar graph of the VSCC of the equilibrium geometry of water. This graph has six vertexes(V), seven edges (E) and three faces (F), representing the (3,−3), (3,−1), and (3,+1) CPs respectively (two faces appear as triangles in the center, the rest of the plane corresponds to the third face). The planar graph formula is obeyed since $V - E + F = 6 - 7 + 3 = 2$. The nonbonding(nb) and bonding(b) maxima (between O and H) form an approximately tetrahedral arrangement. The "H maxima" are almost coincident with the corresponding nuclear positions of the hydrogens.

The structure of a system, in the context of this work, is defined by an *equivalence class* of the VSCC and VSCD graphs. An equivalence class in this case is a set of graphs that can be homeomorphically[3] (i.e., plastically) deformed into one another. This means that the precise positions of the CPs in two graphs do not have to be the same, but they must have identical numbers of each type of CP, and these CPs must be connected in an identical way.

3. Computational Details

All wave functions have been obtained using the Gaussian98 suite of codes.[53] We have employed the B3LYP hybrid density functional method[54] as implemented in Gaussian98, with the 6-311+G(2d,p) basis set.[55] The changing topology of the umbrella inversion was studied within the C_{3v} point group. The reaction coordinate was defined as the angle, α, between the C_3 axis and the hydrogen atoms. At each point along the reaction-path, the remaining internal coordinates were optimized using analytic gradient techniques. As expected the transition-state for the inversion was the D_{3h} geometry with $\alpha = 90°$, whereas the minimum energy structure has $\alpha = 111.66°$ ($r_{NH} = 1.0151$ Å). We have considered the changing topology over a range of values of α, up to 145°, beyond this point the optimum N−H bond-lengths become very long and the structure cannot truly be considered to be a bound ammonia molecule.

The CPs and gradient paths connecting them have been located and traced using the MORPHY01 code.[56] The CPs are found using an eigenvector-following algorithm,[57] the gradient paths are traced[58] using the Burlisch−Stoer ordinary differential equation solver.[59] We have restricted the discussion in this paper to the VSCD and VSCD graphs. 3D pictures were generated using RASMOL[60] and the 2D schematics using Xfig.

4. Full Topology of $L(r)$ and its Change in Ammonia

The electron density of a single ammonia molecule possesses seven CPs: four maxima each virtually coincident with a nucleus, and three bond CPs, each one somewhere between the nitrogen and a hydrogen nucleus. The function $L(\mathbf{r})$ on the other hand shows far more complexity. In the geometries considered in this work, we discovered at least 54 CPs per geometry, whereas Paper I reported 43 CPs in $L(\mathbf{r})$ of the equilibrium geometry of water.

4.1 The VSCC Graphs. The VSCC graph for the transition-state of the "umbrella" inversion of ammonia, $\alpha = 90°$, is shown in Figure 2. As expected, this graph has 3-fold symmetry, which is also observed in all following VSCC and VSCD graphs. The eight maxima in $L(\mathbf{r})$, (3, −3) CPs, fall into three groups: three maxima almost coincident with the coordinates of the hydrogen nuclei, three maxima between the hydrogen nuclei and the nitrogen nucleus (associated with bonding charge concentrations), and two maxima on the C_3 axis, equidistant above and below the molecular plane, which are associated with the nonbonding charge concentrations. A total of nine (3,−1) CPs can be found, each connecting two (3,−3) CPs via a gradient path in $L(\mathbf{r})$. Finally three (3,+1) CPs are found.

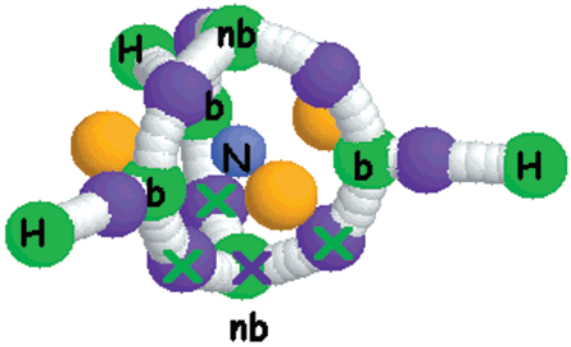

Figure 2. Valence Shell Charge Concentration graph for the transition state in $NH_3(\alpha = 90°)$, associated with VSCC I. There are eight maxima, (3,−3) (green); nine saddle points, (3,−1) (purple); and three minima, (3,+1) (yellow). The gradient paths connecting the (3,−3) and (3,−1) CPs are shown as superpositions of white spheres. The crossed CPs merge as α is increased beyond 106°, leading to the VSCC II graph, which does not contain the lower nonbonding maximum.

The planar graph of the structure shown in Figure 2, labeled VSCC I, is shown in Figure 3a. The vertexes correspond to the (3, −3) CPs, the edges to the (3,−1) CPs and the faces to the (3,+1) CPs. Clearly, the formula $V - E + F = 2$ is obeyed because $8 - 9 + 3 = 2$. This information is repeated in Table 1, which shows that each of the six valence shell graphs occurring in the ammonia inversion obey the $V - E + F = 2$ formula. The planar graph shown in Figure 3a is that of a structure that persists over a fairly large range of α values. In fact, the transition from the structure seen for VSCC I to that of VSCC II only occurs once the deformation parameter α has reached a value of 106°. The doublet of nonbonding maxima was observed before for nitrogen, above and below the symmetry plane of a planar configuration of formamide.[49] That work suggested that the appearance of the doublet of equivalent maxima was a consequence of symmetry, but here we learn that it is a feature even for heavily distorted ammonia, which lacks a mirror plane.

The VSCC graph for ammonia with $\alpha = 120°$ is shown in Figure 4. There are now only seven maxima, three associated with the hydrogen nuclei, three associated with the N−H bonding charge concentrations and *one* associated with the nonbonding charge concentration of the nitrogen nucleus. As with the VSCC I graph, all the maxima are connected via (3,−1) CPs. The second nonbonding maximum of VSCC I has now been replaced by a (3,+1) CP. The mechanism for the transition from VSCC I to VSCC II will be discussed in detail in the next section. The planar graph representation of this structure, labeled VSCC II, is shown in Figure 3b.The planar graph shown in Figure 3b represents a structure that persists over values of α from 106° to 134°.

The VSCC graph for ammonia with $\alpha = 137°$, designated as VSCC III, is shown in Figure 5. The number of maxima is the same as in VSCC II. However, the three CPs associated

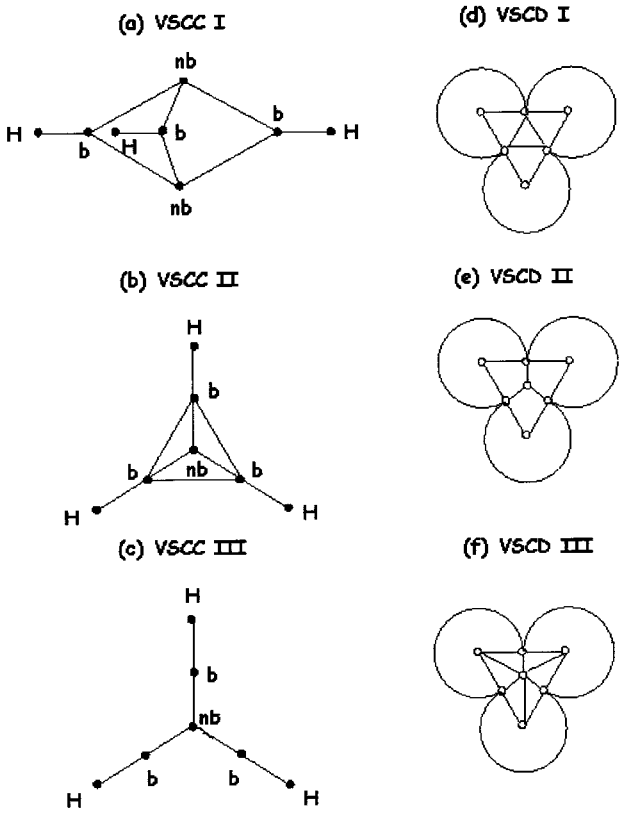

Figure 3. Planar graph representations of the three VSCC graphs (a−c) and the three VSCD graphs (d−f) occurring in the inversion of ammonia. The solid circles (vertexes) in the VSCC graphs represent the (3,−3) CPs, and the edges the (3,−1) CPs. The open circles (vertexes) in the VSCD graphs represent the (3,+3) CPs, and the edges the (3,+1) CPs. Table 1 shows the total number of vertexes, edges, and faces of each graph. Note that the rest of the plane, outside enclosed faces, also represents a face. The edges have been drawn such that they do not cross, as required for planar graphs.

TABLE 1: Survey of the Validity of the Planar Graph Formula ($V - E + F = 2$) for All VSCC and VSCD Graphs, with a Reference to the Figures that Illustrate the Graphs

graph	figures	V	E	F
VSCC I	2, 3a	8	9	3
VSCC II	4, 3b	7	9	4
VSCC III	5, 3c	7	6	1
VSCD I	7, 3d	6	12	8
VSCD II	8, 3e	7	12	7
VSCD III	9, 3f	7	15	10

with the N−H bonding charge concentrations are no longer connected to each other. The graph also has three less (3,+1) CPs. The mechanism for the transition from VSCC II to VSCC III will be discussed in detail in the next section. The planar graph representation of this structure, labeled VSCC III, is shown in Figure 3c. This planar graph represents a structure that persists over values of α from 135° to ∼145°.

4.2 Mechanisms of Transition between VSCC Graphs. The concepts employed in this discussion have all been previously introduced in the consideration of analogous (possibly more complex) transitions of the molecular graphs of the electron density.[2] All transitions in structure are abrupt and discontinuous. The change from VSCC I to VSCC II involves the loss of a (3,−3) CP and the gain of (3,+1) CP, or in terms of the planar graph representation the loss of a vertex and gain of a face. A schematic representation of the transition is given in Figure 6. The arrows show the relative direction of movement of the CPs as the value of α is increased, snapshots of which are shown

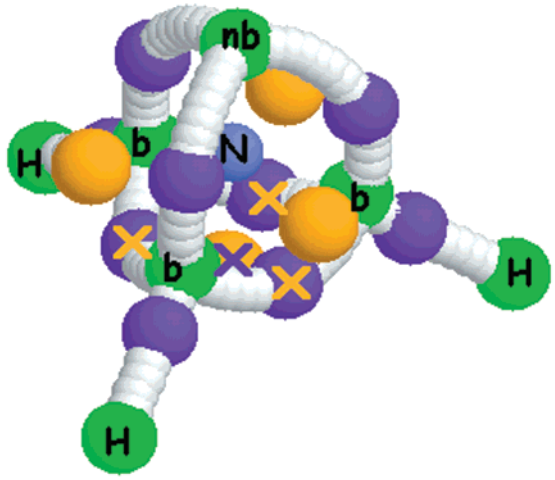

Figure 4. Valence Shell Charge Concentration graph in NH_3 corresponding to α = 120°, associated with VSCC II. There are eight maxima, (3,−3) (green); nine saddle points, (3,−1) (purple); and three minima, (3,+1) (yellow).

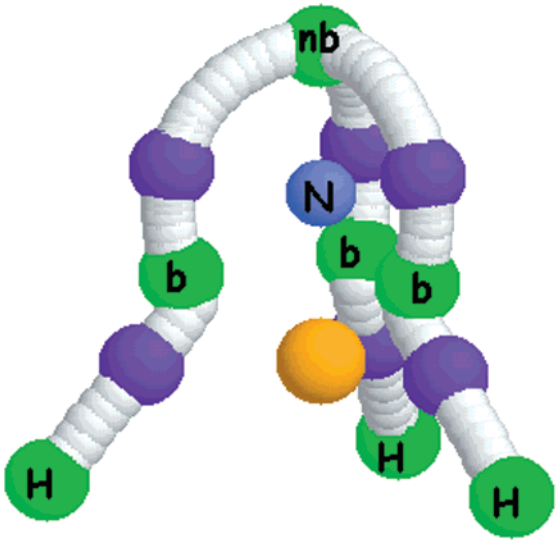

Figure 5. Valence Shell Charge Concentration graph in NH_3 corresponding to α = 135°, associated with VSCC III. There are seven maxima, (3,−3) (green); six saddle points, (3,−1) (purple); and one minimum, (3,+1) (yellow).

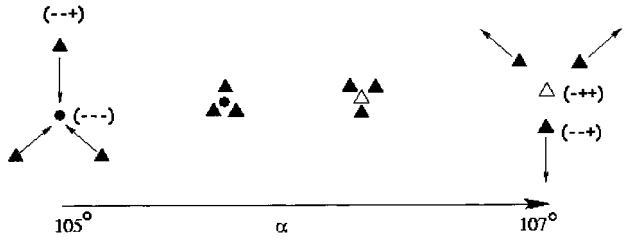

Figure 6. Schematic representation of the mechanism of transition from VSCC I (Figure 2) to VSCC II (Figure 4). Filled triangles represent (3,−1) CPs, filled circles (3,−3) CPs and open triangles (3,+1) CPs. The triplets in brackets indicate the signs of the eigenvalues. The filled triangles in the two diagrams on the left correspond to the crossed purple spheres in Figure 2, whereas the central filled circle corresponds to the crossed green sphere. Similarly, the filled triangles in the two diagrams on the right correspond to the crossed purple spheres in Figure 4, whereas the central open triangle corresponds to the crossed yellow sphere.

going from left to right. As the value of α is increased the three (3,−1) CPs, which connect the N−H bonding maxima to the

second nonbonding (nb) maximum (bottom "nb" in Figure 2), converge upon this nonbonding maximum. This is an example of a bifurcation mechanism (see ref. 3, Chapter 6.). Unlike what is normally seen in the topology of ρ, where it is very common to observe the mutual annihilation of an RCP and a BCP, the transition from VSCC I to VSCC II involves the simultaneous occurrence of three bifurcation mechanisms.

Now we discuss the transition depicted in Figure 6 in terms of the Hessian of $L(\mathbf{r})$, in particular in terms of its (ordered) eigenvalues ($\lambda_1 < \lambda_2 < \lambda_3$), and the associated eigenvectors ($\mathbf{u}_1$, $\mathbf{u}_2$, $\mathbf{u}_3$). The three eigenvalues of the Hessian at the (3,−3) CP which appears in VSCC I (solid circle) are negative, or (−,−,−). The three eigenvalues of the (3,+1) CP in VSCC II (open triangle) that replaces the (3,−3) CP has the following signs (−,+,+). To change from one VSCC I to II two of the eigenvalues must change sign, which can only happen if they become zero. The other eigenvalue, whose numerical value is virtually unchanged during the transition, is associated with an eigenvector perpendicular to the plane of the paper in Figure 6 (i.e., along the C_3 axis). The other two eigenvectors make up an axis system in the plane of the paper. Because of the symmetry of the system, the (3,−3) CP and the three (3,−1) CPs combine at the bifurcation point to leave a doubly degenerate (1,−1) CP. Upon any further infinitesimal increase in the parameter α this degenerate CP generates the (3,+1) CP and three (3,−1) CPs of VSCC II.

The transition from VSCC II to VSCC III is simpler to comprehend than the one just discussed (compare Figures 4 and 5, or Figures 3b and 3c). In this case, there is a loss of three (3,+1) CPs and three (3,−1) CPs. As with the previous transition, the mechanism is of the bifurcation type, but now it is completely analogous to that commonly seen in ρ, where a RCP annihilates a BCP. Here, however, three separate bifurcations occur simultaneously, as each of the three (3,−1) and (3,+1) CP pairs approach and annihilate as the parameter α is increased. The transition from VSCC II to VSCC III appears to be an initial step in the dissociation of ammonia into N and H_3 along this reaction path.

4.3 The VSCD Graphs. The VSCD graph for the transition state of the inversion of ammonia, $\alpha = 90°$, is shown in Figure 7. This graph contains six minima that are connected to each other via 12 (3,+1) CPs. The eight (3,−1) CPs cap the faces of the VSCD graph. From Table 1, we observe that the $V - E + F = 2$ formula is obeyed, provided the vertexes are associated with minima, the edges with (3,+1) CPs and the faces with (3,−1) CPs. When comparing the corresponding VSCC graph in Figure 2 with the current VSCD graph in Figure 7, we observe that each nonbonding maximum (in Figure 2) is capped by a face centered at a (3,−1) CP lying on the C_3 axis.

The planar graph representation of this structure, labeled VSCD I, is shown in Figure 3d. As observed for VSCC I the structure represented by the planar graph of Figure 3e persists for values of α far beyond the planar geometry. The transition from VSCD I to VSCD II occurs around 107.5°, a slightly greater value of α than observed for the equivalent VSCC graphs (106°). This nonsimultaneous transition of the VSCC and VSCD graphs is remarkable.

The VSCD graph for ammonia with $\alpha = 120°$ is shown in Figure 8. This graph contains an additional minimum on the C_3 axis almost in the plane of the hydrogen atoms, below the nitrogen (marked by a cross in Figure 8). The planar graph representation of this structure, labeled VSCD II, is shown in Figure 3e. This graph is representative of the structure found for ammonia with α ranging from 107.5° to 128°. This graph is compatible with VSCC II (Figure 4), which only has a single nonbonding maximum, over a large α interval (see Figure 11). The increase in the number of minima (vertexes) is complemented by a decrease in the number of (3,−1) CPs (faces), as required by the $V - E + F = 2$ rule. The number of (3,+1) CPs (edges) remains the same, connecting all the minima by unique gradient paths.

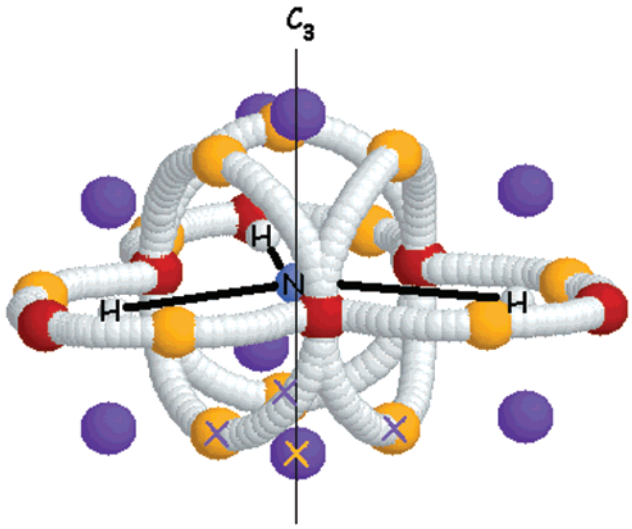

Figure 7. Valence Shell Charge Depletion graph in NH_3 corresponding to $\alpha = 90°$, associated with as VSCD I. For clarity, the ammonia molecule has been marked. There are six minima, (3,+3) (brown), three of which are in the outer region, near the hydrogen nuclei, whereas the other three minima form a triangle around the nitrogen nucleus. The minima in the former subset are each connected twice, whereas the minima in the latter (crossed) subset are each connected six times. There are 12 (3,+1) CPs (yellow, edge) and eight (3,−1) CPs (purple, face). The (3,−1) CPs appear as four doublets, in the vicinity of each nucleus, above and below the mirror plane. The crossed (3,+1) CPs are involved in the transition to VSCD II (see Figure 10).

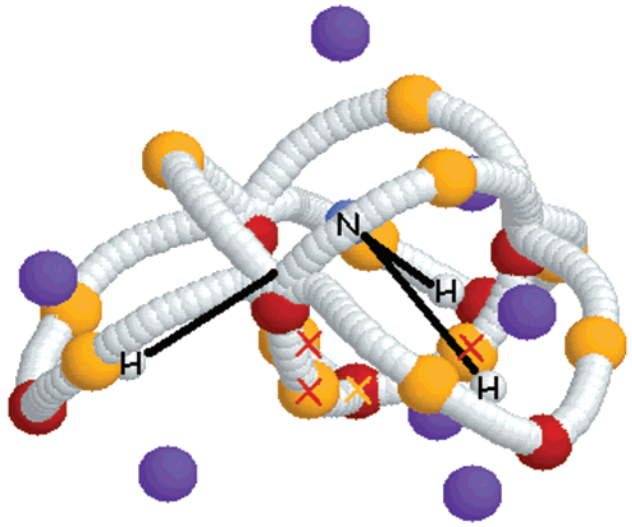

Figure 8. Valence Shell Charge Depletion graph in NH_3 corresponding to $\alpha = 120°$, associated with as VSCD II. For clarity, the ammonia molecule has been marked. This graph has been oriented to optimize the comparison with VSCD I (Figure 7). There are seven minima, (3,+3) (brown); the extra minimum is marked by a cross (see also Figure 3e, where it appears as the central solid square). There are still 12 (3,+1) CPs (yellow, edge) but now only seven (3,−1) CPs (purple, face), compared to VSCD I. Note that six (3,−1) CPs appear as three doublets, in the vicinity of the hydrogen nucleus. One (3,−1) CP appears (purple sphere at the top) above the nitrogen nucleus, on the C_3 axis, which also passes through the crossed minimum at the bottom.

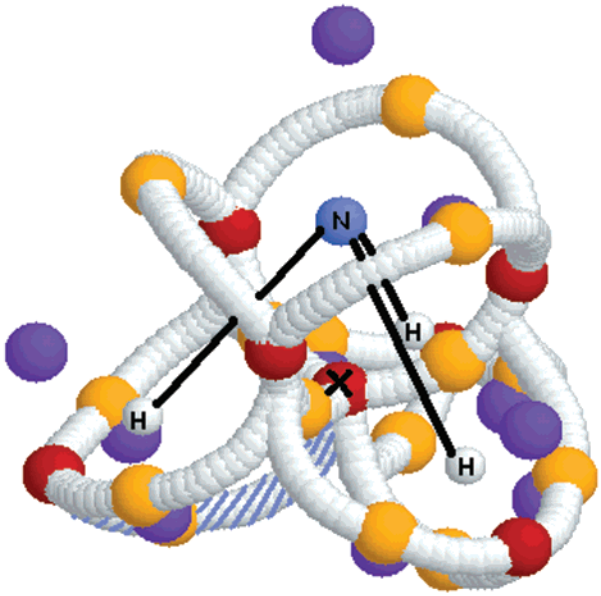

Figure 9. Valence Shell Charge Depletion graph in NH_3 corresponding to $\alpha = 135°$, associated with as VSCD III. For clarity, the ammonia molecule has been marked. This graph has been oriented to optimize the comparison with VSCD II (Figure 8). The minimum (brown sphere) lying on the C_3 axis has been marked by a cross (this same minimum is marked by a cross in Figure 8). This minimum appears as the central solid square in Figure 3e. This minimum is now connected six times, rather than three times as in VSCDII (Figure 8). One such extra gradient path, connecting the crossed minimum to an outer minimum near (and beyond) the hydrogen nucleus is hatched in blue.

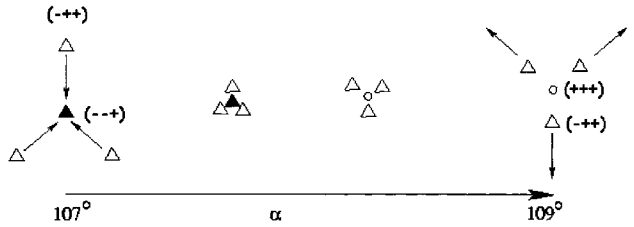

Figure 10. Schematic representation of the transition from VSCD I (Figure 7) to VSCD II (Figure 8). Open circles represent (3,+3) CPs, open triangles (3,+1) CPs and filled triangles (3,−1) CPs. The triplets in brackets indicate the signs of the eigenvalues. The arrows show the relative direction of movement of the CPs as the value of α is increased, snapshots of which are shown going from left to right. The open triangles on the two diagrams on the left correspond to the three crossed yellow spheres in Figure 7, whereas the central filled triangle corresponds to the crossed purple sphere. Similarly, the open triangles in the two diagrams on the right correspond to the crossed yellow spheres in Figure 8, whereas the central open circle corresponds to the crossed brown sphere.

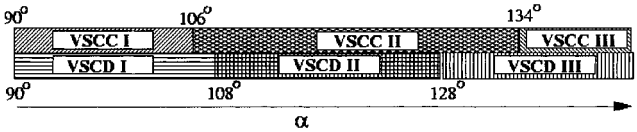

Figure 11. Survey of the appearance of the three Valence Shell Charge Concentrations graphs (VSCC I, VSCC II, VSCC III) and the three Valence Shell Charge Depletion graphs (VSCD I, VSCD II, VSCD III) in terms of the angle intervals of the control parameter α.

The VSCD graph for ammonia at $\alpha = 137°$ is shown in Figure 9. The planar graph representation of this structure, labeled VSCD III, is given in Figure 3f. This graph contains the same number of minima as the VSCD II graph, and is common to structures found for geometries from 128° to ∼145°. The number of (3,+1) (edges) and (3,−1) CPs (faces) are both increased by three (see Table 1). The new (3,+1) CPs lie on gradient paths connecting the minimum on the C_3 axis (brown sphere marked by a cross in Figure 9), to the outlying minima, beyond the hydrogen atoms. For clarity one such gradient path is hatched in blue.

Knowledge of the connectivity in the graphs allows a definitive allocation of the (3,−1) and (3,+1) CPs to either the charge concentration or depletion graphs. The (3,−1) CPs that connect two (3,−3) CPs belong to the charge concentration graph (see for example Figure 2). The (3,−1) CPs that have a path to infinity belong to the charge depletion graph. The (3,+1) CPs that connect two valence (3,+3) CPs belong to the charge depletion graph (see for example Figure 7). The (3,+1) CPs that connect to core−shell-(3,+3)-CPs belong to the charge concentration graph. Making these assignations is vital if we want to disentangle the graphs and successfully apply the $V - E + F = 2$ rule that governs planar graphs. Note that the (3,−1) CPs are counted as edges or faces depending on whether they belong to the VSCC or VSCD graphs, respectively. Equally (3,+1) CPs are counted as faces or edges if they are part of the VSCC or VSCD graphs, respectively. In this sense, one could view the VSCC and VSCD as dual.

4.4 Mechanisms of Transition between VSCD Graphs. The change from VSCD I to VSCD II involves the gain of a (3,+3) CP and the loss of a (3,−1) CP, or in terms of the planar graph representation the gain of a vertex and loss of a face. A schematic representation of the transition is given in Figure 10. As the value of α is increased the three (3,+1) CPs that connect the three inner minima, converge upon the lower (3,−1) CP. This process is made clear in Figure 7, where the three crossed yellow spheres mark the (3,+1) CPs, and the crossed purple sphere at the bottom marks the (3,−1) CP. It is instructive to compare Figures 6 and 10 because then the analogy between the VSCC I → VSCC II transition and the VSCD I → VSCD II transition becomes obvious. This comparison again stresses the dual relationship between VSCC and VSCD.

Overall, the transition from VSCD II to VSCD III involves the creation of three edges, (3,+1) CPs, and three faces, (3,−1) CPs. In the electron density, this transition commonly occurs when a ring is formed, only here, it happens in 3-fold because of the symmetry (see ref. 3, p 88). A glance at Figure 3 suggests that, overall, the same type of 3-fold "face creation" is occurring in the transition VSCC III → VSCC II. In other words, when going from regime II to regime III, three faces are annihilated in the concentration region, whereas three faces are created in the depletion region. This change proceeds via the simultaneous conversion of three (3,−1) CPs, each into a (3,+1) CP and two (3,−1) CPs.

5. Discussion

One of the main conclusions of paper I is corroborated here, namely that $L(\mathbf{r})$ possesses an extensive set of connected CPs, which can be subdivided into meaningful graphs. An intriguing question that prompted this contribution is the representation by $L(\mathbf{r})$ of nitrogen's lone-pair in twisted amides. This work explains the mechanism of change in the CP pattern in going from a planar to a pyramidal nitrogen environment, but we need to understand better how a lone pair is associated with a maximum in $L(\mathbf{r})$.

In general, the electron density in a valence region is the result of contributions from many electron pairs.[29] The average pair population of the nonbonding pair on N in NH_3 is 2.9.[61] In view of the strong pair condensation in the core region of non-hydrogen atoms,[61] it is justified to consider a set of only eight (=$\{7 - 2\} + \{3 \times 1\}$) valence electrons in ammonia, which

can form $8 \times (8-1)/2 = 28$ distinct electron pairs. Hence, an average pair population of almost 3 is far below that obtained from a distribution with a random pairing of electrons throughout ammonia.[29] Therefore, it would be wrong to view the nonbonding density on N as originating from a single spatially localized electron pair. Rather this "lone-pair" is an example of a region where the pairing is greatly reduced from the random level. The function $L(\mathbf{r})$ detects this partial pair condensation and thus exhibits at least one maximum in the VSCC near the nitrogen nucleus. From this discussion, we learn that it would be naive to associate one maximum in $L(\mathbf{r})$ with a single well-localized electron pair. Instead, we observe that as the pyramidal nitrogen is flattened a new maximum suddenly emerges from a (3,+1) CP (and a concomitant rearrangement of (3,−1) CPs). This process indicates that the flattening creates a second concentration of nonbonding density, which will eventually develop into the lone-pair. So during the inversion process, there is a stage where two maxima coexist, at both sides of the nitrogen. One would expect a population build-up into the nonbonding zones to accommodate the existence of two maxima as the "umbrella is opened". A previous study[38] on NH_3 using ELF does indeed show that about 0.5e is transferred from the bonding to the nonbonding zone upon flattening of ammonia.

An early study[62] on molecular structure made clear that a structural change inducing a change in the number and type CPs, the system must pass through a bifurcation point.[3] This term is part of catastrophe theory,[63] which was introduced into the topology of electron densities in the early 80s. A full description of the structural changes observed in this work in terms of catastrophe theory would require a separate paper. It suffices to mention here that three types of elementary catastrophes in Thom's classification[2,40] feature in the inversion of ammonia.[38] They are the "elliptic umbillic" in the VSCC I → VSCC II and the VSCD I → VSCD II transition, a triple "fold catastrophe" in the VSCC II → VSCC III transition and a triple "dual cusp" in VSCD II → VSCD III.

It is useful to remember that the (3, +3) CPs are minima in $L(\mathbf{r})$, i.e., regions of minimum local charge concentration, but maxima in the Laplacian, i.e., regions of maximum local charge depletion. The open infinite space surrounding the free ammonia acts as a global attractor for gradient paths in $L(\mathbf{r})$. This situation is the opposite of that occurring in ρ where infinity acts as a global repellor, i.e., a source of gradient paths. This difference is due to the way the scalar function approaches zero at infinity. The electron density asymptotically approaches zero from above, because it is everywhere positive, whereas $L(\mathbf{r})$ approaches zero from below, whereas it is negative in the outer regions, where charge depletion rules.

We close with a brief discussion of the Poincaré-Hopf relationship,[2,64] which can be viewed as a generalization of the $V - E + F = 2$ formula. The Poincaré−Hopf relationship enables one to check the consistency of a set of CPs in general, irrespective of its potential division into planar subgraphs. Because at infinity $L(\mathbf{r})$ approaches zero as a negative function the Poincaré−Hopf relationship becomes

$$n(3,-3) - n(3,-1) + n(3,+1) - n(3,+3) = -1 \quad (2)$$

where $n(3,m)$ is the number of $(3,m)$ CPs ($m = -3,-1,+1,+3$). As an example, we test eq 2 on the full structure of $\alpha = 90°$. In that case, the CSCD has three (3,+3) CPs, three (3,+1) CPs, and two (3,−1) CPs, such that $V - E + F = 3 - 3 + 2 = 2$. The CSCC consists of only one (3,−3) CP. Adding the CP count of VSCC I and VSCD I given in Table 1 to this information yields that $n(3,-3) - n(3,-1) + n(3,-3) - n(3,-3) = 9 - 19 + 18 - 9 = -1$.

Finally, it should be noted that the VSCC I → VSCC II transition is analogous to the transition in ELF as reported by Krokidis et al.[38] The transition in ELF occurs at 105.2° and in $L(\mathbf{r})$ at 106° (Figure 11), which is remarkably similar given the uncertainty in the level of calculation.

6. Conclusion

For the first time, dynamic changes in the topology of $L(\mathbf{r})$ are reported in detail, building on work that considered the static full topology of $L(\mathbf{r})$ in water. In this work, the nuclear skeleton of the test case ammonia is controlled by an angle α, which preserves the 3-fold symmetry. This parameter describes the well-known NH_3 inversion, and distorts the geometry over a considerable range from the planar transition state to a geometry far beyond the equilibrium geometry. More than 50 critical points in $L(\mathbf{r})$ are discerned but based on the network of connecting gradient paths they can be subdivided into graphs. These sub-networks extend over the whole molecule and can be represented by planar graphs. Three VSCC graphs and three VCSD graphs are discerned, each associated with a range of stability of at least ∼15°in α. The transitions between the VSCC graphs do not occur at the same α values as the transition between the VSCD graphs. We have elucidated how lone pairs are presented by $L(\mathbf{r})$ under inversion, thereby providing a valuable complement to studies based on ELF.

References and Notes

(1) Popelier, P. L. A.; Aicken, F. M.; O'Brien, S. E. In *Chemical Modelling: Applications and Theory*; *Royal Society of Chemistry Specialist, Periodical Report, Chapter 3, pp.143-198;* Hinchliffe, A., Ed.; Royal Society of Chemistry: 2000; Vol. 1; pp 143−198.

(2) Bader, R. F. W. *Atoms in Molecules. A Quantum Theory*; Oxford University Press: 1990.

(3) Popelier, P. L. A. *Atoms in Molecules. An Introduction*; Pearson Education: Harlow, UK, 2000.

(4) Bader, R. F. W.; Beddall, P. M. *J. of Chem. Phys.* **1972**, *56*, 3320.

(5) Becke, A. D.; Edgecombe, K. E. *J. Chem. Phys.* **1990**, *92*, 5397.

(6) Popelier, P. L. A. *Mol. Phys.* **1996**, *87*, 1169.

(7) Popelier, P. L. A. *Comput. Phys. Commun.* **1998**, *108*, 180.

(8) Popelier, P. L. A.; Kosov, D. S. *J. Chem. Phys.* **2001**, *114*, 6539.

(9) Keith, T. A.; Bader, R. F. W.; Aray, Y. *Intern. J. Quantum Chem.* **1996**, *57*, 183.

(10) Keith, T. A.; Bader, R. F. W. *J. Chem. Phys.* **1993**, *99*, 3669.

(11) Cioslowski, J.; Liu, G. H. *J. Chem. Phys.* **1999**, *110*, 1882.

(12) Schmider, H. L.; Becke, A. D. *J. Mol. Struct. (THEOCHEM)* **2000**, *527*, 51.

(13) Gillespie, R. J.; Bayles, D.; Platts, J.; Heard, G. L.; Bader, R. F. W. *J. Phys. Chem. A* **1998**, *102*, 3407.

(14) Bader, R. F. W.; MacDougall, P. J.; Lau, C. D. H. *J. Am. Chem. Soc.* **1984**, *106*, 1594.

(15) Bader, R. F. W.; MacDougall, P. J. *J. Am. Chem. Soc.* **1985**, *107*, 6788.

(16) Carroll, M. T.; Chang, C.; Bader, R. F. W. *Mol. Phys.* **1988**, *63*, 387.

(17) Bader, R. F. W.; Chang, C. *J. Phys. Chem.* **1989**, *93*, 2946.

(18) Carroll, M. T.; Cheeseman, J. R.; Osman, R.; Weinstein, H. *J. Phys. Chem.* **1989**, *93*, 5120.

(19) Bader, R. F. W.; Popelier, P. L. A.; Chang, C. *Theochem- J. Mol. Struct.* **1992**, *87*, 145.

(20) Gillespie, R. J. *Struct. Chem.* **1998**, *9*, 73.

(21) Gillespie, R. *Can. J. Chem.* **1992**, *70*, 742.

(22) Gillespie, R. J. *Molecular Geometry*; Van Nostrand Reinhold: London, 1972.

(23) Gillespie, R. J.; Hargittai, I. *The VESPR Model of Molecular Geometry*; Allyn & Bacon and Prentice Hall: Boston, US, 1991.

(24) Fradera, X.; Austen, M. A.; Bader, R. F. W. *J. Phys. Chem. A* **1999**, *103*, 304.

(25) Bytheway, I.; Gillespie, R. J.; Tang, T. H.; Bader, R. F. W. *Inorg. Chem.* **1995**, *34*, 2407.

(26) Gillespie, R. J.; Bytheway, I.; Dewitte, R. S.; Bader, R. F. W. *Inorg. Chem.* **1994**, *33*, 2115.

(27) Bader, R. F. W.; Gillespie, R. J.; Martin, F. *Chem. Phys. Lett.* **1998**, *290*, 488.
(28) Bytheway, I.; Popelier, P. L. A.; Gillespie, R. J. *Can. J. Chem.* **1996**, *74*, 1059.
(29) Bader, R. F. W.; Heard, G. L. *J. Chem. Phys.* **1999**, *111*, 8789.
(30) Silvi, B.; Savin, A. *Nature(London)* **1994**, *371*, 683.
(31) Savin, A.; Silvi, B.; Colonna, F. *Can. J. Chem.* **1996**, *74*, 1088.
(32) Noury, S.; Colonna, F.; Savin, A.; Silvi, B. *J. Mol. Struct.* **1998**, *450*, 59.
(33) Fuster, F.; Silvi, B. *Theor. Chem. Acc.* **2000**, *104*, 13.
(34) Fuster, F.; Silvi, B. *Chem. Phys.* **2000**, *252*, 279.
(35) LLusar, R.; Beltran, A.; Andres, J.; Noury, S.; Silvi, B. *J. Comput.Chem.* **1999**, *20*, 1517.
(36) Silvi, B.; Gatti, C. *J. Phys. Chem. A* **2000**, *104*, 947.
(37) Joubert, L.; Silvi, B.; Picard, G. *Theor. Chem. Acc.* **2000**, *104*, 109.
(38) Krokidis, X.; Noury, S.; Silvi, B. *J. Phys. Chem. A* **1997**, *101*, 7277.
(39) Tal, Y.; Bader, R. F. W.; Erkku, J. *Phys. Rev. A* **1980**, *21*, 1.
(40) Thom, R. *Structural Stability and Morphogenesis*; English ed.; Benjamin: Reading, MA, 1975.
(41) Krokidis, X.; Vuilleumier, R.; Borgis, D.; Silvi, B. *Mol. Phys.* **1999**, *96*, 265.
(42) Fuster, F.; Sevin, A.; Silvi, B. *J. Phys. Chem. A* **2000**, *104*, 852.
(43) Berski, S.; Silvi, B.; Latajka, Z.; Leszczynski, J. *J. Chem. Phys.* **1999**, *111*, 2542.
(44) Beltran, A.; Andres, J.; Noury, S.; Silvi, B. *J. Phys. Chem.* **1999**, *103*, 3078.
(45) Krokidis, X.; Silvi, B.; Alikhani, M. E. *Chem. Phys. Lett.* **1998**, *292*, 35−45.
(46) Krokidis, X.; Silvi, B.; Dezarnaud-Dandine, C.; Sevin, A. *New. J. Chem.* **1998**, 1341.
(47) Popelier, P. L. A. *Coord. Chem. Rev.* **2000**, *197*, 169.
(48) Hernandez-Trujillo, J.; Bader, R. F. W. *J. Phys. Chem. A.* **2000**, *104*, 1779.
(49) Laidig, K. E.; Bader, R. F. W. *J. Am. Chem. Soc.* **1991**, *113*, 6312.
(50) Bader, R. F. W.; Gillespie, R. J.; MacDougall, P. J. *J. Am. Chem. Soc.* **1988**, *110*, 7329.
(51) Trinajstic, N. *Chemical Graph Theory*; CRC: Boca Raton, Florida, US, 1983; Vol. 1.
(52) Bader, R. F. W.; Nguyen-Dang, T. T.; Tal, Y. *Rep. Prog. Phys.* **1981**, *44*, 893.
(53) Frisch, M. J.; Trucks, G. W.; Schlegel, H. B.; Scuseria, G. E.; Robb, M. A.; Cheeseman, J. R.; Zakrzewski, V. G.; Montgomery, J. A., Jr.; Stratmann, R. E.; Burant, J. C.; Dapprich, S.; Millam, J. M.; Daniels, A. D.; Kudin, K. N.; Strain, M. C.; Farkas, O.; Tomasi, J.; Barone, V.; Cossi, M.; Cammi, R.; Mennucci, B.; Pomelli, C.; Adamo, C.; Clifford, S.; Ochterski, J.; Petersson, G. A.; Ayala, P. Y.; Cui, Q.; Morokuma, K.; Malick, D. K.; Rabuck, A. D.; Raghavachari, K.; Foresman, J. B.; Cioslowski, J.; Ortiz, J. V.; Stefanov, B. B.; Liu, G.; Liashenko, A.; Piskorz, P.; Komaromi, I.; Gomperts, R.; Martin, R. L.; Fox, D. J.; Keith, T.; Al-Laham, M. A.; Peng, C. Y.; Nanayakkara, A.; Gonzalez, C.; Challacombe, M.; Gill, P. M. W.; Johnson, B. G.; Chen, W.; Wong, M. W.; Andres, J. L.; Head-Gordon, M.; Replogle, E. S.; Pople, J. A. *Gaussian 98*, revision A.7; Gaussian, Inc.: Pittsburgh, PA, 1998.
(54) Becke, A. D. *J. Chem. Phys.* **1993**, *98*, 5648.
(55) Krishnan, R.; Binkley, J. S.; Seeger, R.; Pople, J. A. *J. Chem. Phys.* **1980**, *72*, 650.
(56) MORPHY01, A program written by P. L. A. Popelier with a contribution from R. G. A. Bone, D.Kosov, M.in het Panhuis, UMIST, Manchester, England, EU 2001.
(57) Popelier, P. L. A. *Chem. Phys. Lett.* **1994**, *228*, 160.
(58) Malcolm, N. O. J.; Popelier, P. L. A. unpublished results.
(59) Press, W. H.; Flannery, B. P.; Teucholsky, S. A.; Vetterling, W. T. *Numerical Recipes*, 2nd ed.; Cambridge University Press: Cambridge, 1992.
(60) Sayle, R.; Glaxo-Wellcome, Stevenage, UK, 1994.
(61) Bader, R. F. W.; Stephens, M. E. *J. Am. Chem. Soc.* **1975**, *97*, 7391.
(62) Bader, R. F. W.; Nguyen-Dang, T. T.; Tal, Y. *J. Chem. Phys.* **1979**, *70*, 4316.
(63) Gilmore, R. *Catastrophe Theory for Scientist and Engineers*; Wiley: New York, 1981.
(64) Collard, K.; Hall, G. G. *Int. J. Quantum Chem.* **1977**, *12*, 623.